26. Needham, J. V., Chen, T. Y. & Falke, J. J. Novel ion specificity of a carboxylate cluster Mg(II) binding site: strong charge selectivity and weak size selectivity. *Biochemistry* **32,** 3363–3367 (1993).
27. Flatman, P. W. Mechanisms of magnesium transport. *Annu. Rev. Physiol.* **53,** 259–271 (1991).
28. Horovitz, A. & Fersht, A. R. Strategy for analysing the co-operativity of intramolecular interactions in peptides and proteins. *J. Mol. Biol.* **214,** 613–617 (1990).
29. Koradi, R., Billeter, M. & Wuthrich, K. MOLMOL: a program for display and analysis of macromolecular structures. *J. Mol. Graph.* **14,** 51–55 (1996).

Supplementary Information accompanies the paper on *Nature*'s website (http://www.nature.com/nature).

Acknowledgements

The mSlo1 and mSlo3 clones were provided by L. Salkoff. We thank S. Chen, S. W. Jones and R. Aldrich for comments on the manuscript. This work was supported by grants from the NIH (to J.Q. and J.C.), the American Heart Association and the Whitaker Foundation (to J.C.).

Competing interests statement

The authors declare that they have no competing financial interests.

Correspondence and requests for materials should be addressed to J.C. (e-mail: jxc93@cwru.edu).

Multiple regulatory sites in large-conductance calcium-activated potassium channels

Xiao-Ming Xia, Xuhui Zeng & Christopher J. Lingle

Department of Anesthesiology, Washington University School of Medicine, Box 8054, St. Louis, Missouri 63110, USA

Large conductance, Ca^{2+}- and voltage-activated K^+ channels (BK) respond to two distinct physiological signals—membrane voltage and cytosolic Ca^{2+} (refs 1, 2). Channel opening is regulated by changes in Ca^{2+} concentration spanning 0.5 μM to 50 mM (refs 2–5), a range of Ca^{2+} sensitivity unusual among Ca^{2+}-regulated proteins. Although voltage regulation arises from mechanisms shared with other voltage-gated channels[6–8], the mechanisms of Ca^{2+} regulation remain largely unknown. One potential Ca^{2+}-regulatory site, termed the 'Ca^{2+} bowl', has been located to the large cytosolic carboxy terminus[9–11]. Here we show that a second region of the C terminus, the RCK domain (regulator of conductance for K^+ (ref. 12)), contains residues that define two additional regulatory effects of divalent cations. One site, together with the Ca^{2+} bowl, accounts for all physiological regulation of BK channels by Ca^{2+}; the other site contributes to effects of millimolar divalent cations that may mediate physiological regulation by cytosolic Mg^{2+} (refs 5, 13). Independent regulation by multiple sites explains the large concentration range over which BK channels are regulated by Ca^{2+}. This allows BK channels to serve a variety of physiological roles contingent on the Ca^{2+} concentration to which the channels are exposed[14,15].

A recent advance in understanding the regulation of BK channels by Ca^{2+} was the demonstration that distinct, independent binding sites for Ca^{2+} may explain the range of intracellular Ca^{2+} concentration ($[Ca^{2+}]_i$) that regulates channel opening[5,13]. Over the physiological range of $[Ca^{2+}]_i$, relatively Ca^{2+}-selective site(s) mediate channel regulation. In contrast, the effects of $[Ca^{2+}]_i$ in the millimolar range reflect a lower sensitivity site showing selectivity for Ca^{2+} and Mg^{2+}. Here we define principal structural elements required for each Ca^{2+}-dependent regulatory effect. BK channel α-subunits are encoded by a single *Slo1* gene[16,17], with a functional channel arising from the tetrameric assembly of four α-subunits[18]. Although the transmembrane segments (S1–S6, Fig. 1a) of each α-subunit[17,19] share homology with voltage-gated K^+ channels, each α-subunit uniquely contains an extensive C terminus with four additional hydrophobic segments (S7–S10). The C terminus is probably composed of two modular units, as expression in oocytes of separate messages for S0–S8 and S9–S10 peptides produces channels identical to wild-type BK channels[20]. Whereas the Ca^{2+} bowl is contained within the S9–S10 peptide, the C-terminal structure with the S7–S8 segments contains the RCK domain, a second potential regulatory element (Fig. 1a, b) that exhibits extensive homology with a number of bacterial K^+ channels. The structures of two prokaryotic RCK domains have been determined[12,21] and RCK domains may contain binding sites for a variety of regulatory ligands, including nucleotides[22] and cations[21].

To address the role of the RCK domain in BK channel regulation, we took advantage of the fact that a homologue of *Slo1*, the *Slo3* pH-sensitive K^+ channel, lacks Ca^{2+}-dependent regulation[13,23,24]. We focused on residues near folds in the RCK domain that contribute to nucleotide binding in prokaryotic homologues (Fig. 1c). We were

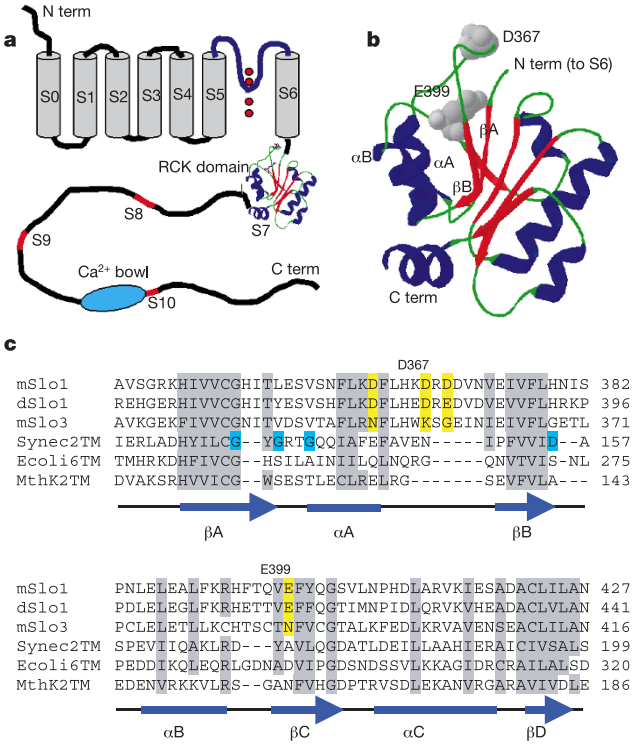

Figure 1 Schematic representation of the Slo1 α-subunit. **a**, The Slo1 α-subunit shares a common transmembrane topology (S1–S6) with voltage-dependent K^+ channels, and contains a unique amino-terminal S0 segment and an extensive cytosolic C-terminal elaboration with hydrophobic segments S8–S10 (red), the Ca^{2+} bowl, and the RCK domain. Segment S7 is contained in the RCK structure[12]. **b**, Structural approximation of the BK channel RCK domain based on the RCK domain of the *E. coli* K^+ channel[12]. The position of the linker between helix αA and βB is uncertain. **c**, Sequence alignment within the RCK domain of Slo1 and Slo3 subunits and three bacterial K^+ channels[12]. Grey indicates semi-conserved residues; blue shows the NAD-binding motif present in some bacterial homologues; and yellow indicates negative residues in *Slo1* that are non-conserved in *Slo3*. mSlo1, mouse BK channel, *Mus musculus* (GenBank accession number: 6754435); dSlo1; *Drosophila* BK channel, *D. melanogaster* (GenBank accession number: 7301192); mSlo3, mouse Slo3 channel, *M. musculus* (GenBank accession number: 6680542); Synec2TM, *Synetchocystis* sp. (GenBank accession number: 7447543); Ecoli6TM, *E. coli* (GenBank accession number: 400124); MthK2TM, *M. thermautotrophicum* (GenBank accession number: 2622639).

particularly interested in negatively charged residues conserved in Ca^{2+}-dependent forms of *Slo1* (for example, *Drosophila* and mouse *Slo1* (*dSlo1* and *mSlo1*, respectively)), but not in *Slo3*. To assess whether a construct exhibits altered Ca^{2+}-dependent gating, we examined the activation characteristics over a range of $[Ca^{2+}]_i$ and $[Mg^{2+}]_i$. In accordance with allosteric models of BK channel activation[4,5,7,13], this approach reveals to what extent a structural alteration influences divalent cation binding, movement of the voltage sensors, or the closed–open conformational equilibria.

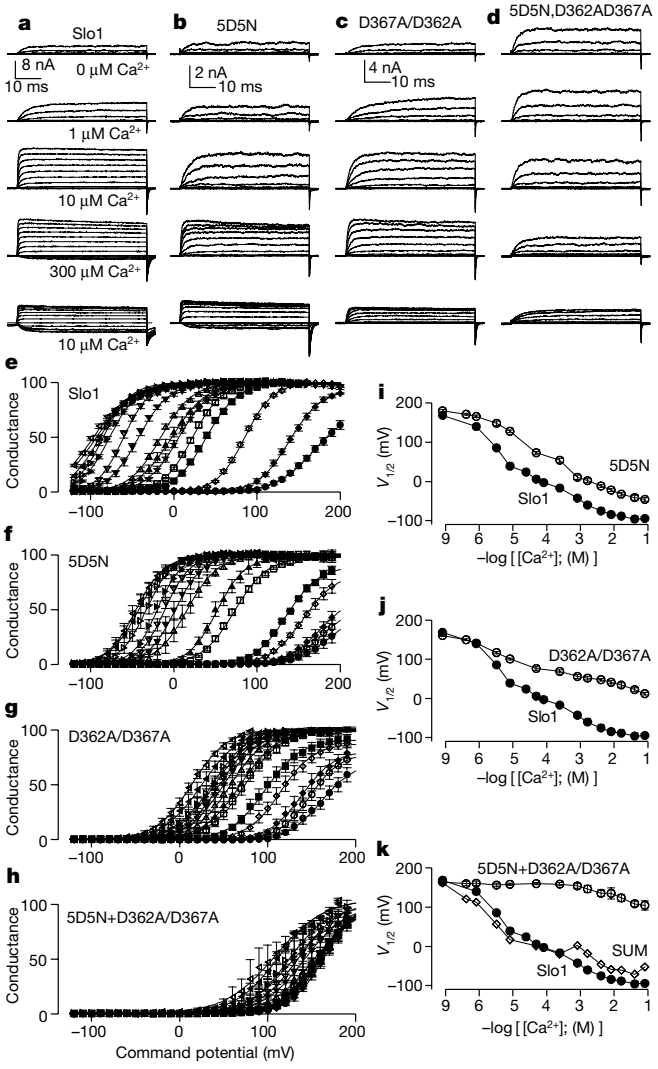

Figure 2 The Ca^{2+} bowl and D362A/D367A account for all physiologically relevant Ca^{2+}-dependent regulation of BK channels. **a**–**d**, Traces show currents from inside-out patches for Slo1, 5D5N, D362A/D367A and the combined mutation 5D5N + D362A/D367A with cytosolic $[Ca^{2+}]_i$ as shown. Voltage steps were from −100 through to +160 in 20-mV increments following 40 ms at −180 mV, with tail currents at −120 mV. **e**–**h**, G–V curves were generated over $[Ca^{2+}]_i$ from 0 to 100 mM for *Slo1* and the indicated mutants. Solid lines are fits of equation (1) (see Methods). $[Ca^{2+}]_i$ are: filled circles, 0 μM; open circles, 0.5 μM; filled diamonds, 1 μM; open diamonds, 4 μM; filled squares, 10 μM; open squares, 60 μM; stars, 100 μM; filled triangles, 300 μM; open triangles, 1 mM; filled triangles (inverted), 2 mM; open triangles (inverted), 5 mM; filled triangles (facing right), 10 mM; open triangles (facing right), 20 mM; filled triangles (facing left), 50 mM; open triangles (facing left), 100 mM. **i**, Activation $V_{1/2}$ versus $[Ca^{2+}]_i$ for wild-type BK currents and for mutation 5D5N. **j**, **k**, Wild-type (*Slo1*) versus D362A/D367A (**j**) and wild-type versus combined mutation of the Ca^{2+} bowl and (**k**, 5D5N + D362A/D367A). The $V_{1/2}$ shift predicted for the case in which the Ca^{2+} bowl and D362A/D367A each independently regulate gating is also shown (SUM).

We first compared the Ca^{2+} sensitivity of wild-type BK currents arising from Slo1 α-subunits to that arising from Slo1 subunits with a mutated Ca^{2+} bowl region (5D5N; see Methods). This mutation abolishes function of the Ca^{2+} bowl[9,11]. Currents resulting from the 5D5N construct still exhibit substantial regulation by Ca^{2+}, although the ability of $[Ca^{2+}]_i$ at less than 10 μM to cause channel activation is reduced relative to wild-type currents (Fig. 2a, b). As seen in a comparison of conductance–voltage (*G*–*V*) curves (Fig. 2e, f), both constructs exhibit similar activation in the absence of Ca^{2+}, but $[Ca^{2+}]_i$ below 10 μM has less effect in the 5D5N construct.

We next examined whether the RCK domain contributes to Ca^{2+}-dependent regulation of current that persists after mutation of the Ca^{2+} bowl. Of the prokaryotic channels containing an RCK domain, only some contain the conserved motif between β-sheet A and α-helix B (Fig. 1c) that defines nucleotide binding[22]. This region of Slo1 and Slo3 exhibits no obvious residues that might account for a difference in Ca^{2+} sensitivity. However, at the end of αA and through the linker up to βB, there are three aspartate residues (D362, D367 and D369 in mSlo1) conserved in Slo1 forms, but which are neutral or positively charged in Slo3. Compared with bacterial homologues[12], the linker between αA and βB in the *Slo* family of subunits contains five extra residues (Fig. 1c), suggesting an important functional role for this segment.

The point mutations D362A and D369A each resulted in currents with Ca^{2+} sensitivity similar to wild-type currents, with a slight effect of D362A at lower $[Ca^{2+}]_i$. In contrast, D367A produced a marked reduction in the ability of Ca^{2+} to shift gating. Constructs D362A/D367A and D362A/D367A/D369A exhibited behaviour similar to D367A alone. We focused on the D362A/D367A double mutant. Currents arising from D362A/D367A exhibited reduced Ca^{2+}-dependent regulation of activation (Fig. 2c). The resulting *G*–*V* curves (Fig. 2g) show that the full shift in gating over all $[Ca^{2+}]_i$ with the D362A/D367A mutation is less than that in 5D5N, although D362A/D367A exhibits more sensitivity to $[Ca^{2+}]_i$ below 10 μM (Fig. 2f, g). When both the Ca^{2+} bowl and RCK

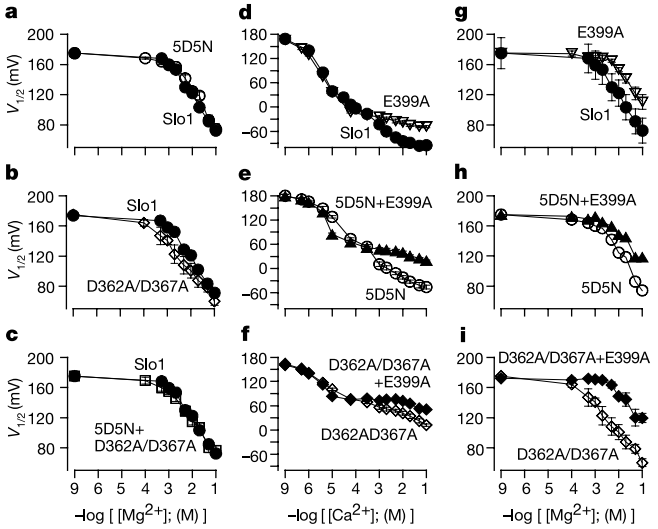

Figure 3 The RCK domain also mediates effects of high concentrations of Ca^{2+} and Mg^{2+}. **a**–**c**, $V_{1/2}$ as a function of $[Mg^{2+}]_i$ for pairs of site mutations. **d**–**f**, $V_{1/2}$ as a function of $[Ca^{2+}]_i$ for different mutations with and without E399A. **g**–**i**, $V_{1/2}$ as a function of $[Mg^{2+}]_i$ for different mutations with and without E399A. *Slo1* is indicated by filled circles. $V_{1/2}$ shifts resulting from changing $[Ca^{2+}]_i$ from 1 to 100 mM: Slo1, 51.5 ± 2.4 mV; plus E399A*, 22.3 ± 1.5 mV; 5D5N, 62.2 ± 4.9 mV, plus E399A**, 26.0 ± 3.5 mV; D362A/D367A, 48.0 ± 3.9 mV, plus E399A, 23.5 ± 5.5 mV. $V_{1/2}$ shifts for 0–100 mM $[Mg^{2+}]_i$: *Slo1*, 109.8 ± 2.8 mV, plus E399A**, 63.9 ± 6.6 mV; 5D5N, 108.9 ± 5.6 mV, plus E399A*, 56.7 ± 4.3; D362A/D367A, 112.0 ± 4.2 mV, plus E399A*, 75.5 ± 6.3 mV. Asterisk, $P < 0.001$; double asterisk, $P < 0.002$.

domain residues were mutated simultaneously (5D5N plus D362A/D367A), the channels were still gated by voltage in a fashion similar to wild-type currents, but Ca^{2+} had essentially no effect on gating at concentrations up to 1 mM (Fig. 2d, h). Together, the loci defined by 5D5N and D362A/D367A account for all Ca^{2+}-dependent regulation of BK channels over the physiologically important range of $[Ca^{2}]_i$.

For BK currents, the voltage of half activation ($V_{1/2}$) of conductance at different $[Ca^{2+}]_i$ provides a useful indicator of the apparent Ca^{2+}-dependence of activation. For all four constructs, the $V_{1/2}$ for activation at 0 Ca^{2+} remained within 20 mV of each other (Fig. 2i–k), indicative that these mutations were not altering strictly voltage-dependent equilibria. Allosteric models predict that, if two loci reflect the independent contribution of two Ca^{2+}-regulatory elements, the magnitude of the shifts in $V_{1/2}$ resulting from the effects of each individual site should sum to be similar to the effect of the combined mutation[5,7,13] (equation (3); see also Methods). Therefore, we summed the residual shift in $V_{1/2}$ after mutation of both sites with the increments in $V_{1/2}$ attributable to the Ca^{2+} bowl and to the D362/D367 site (Fig. 2k, open diamonds). The correspondence between wild-type values of $V_{1/2}$ and those predicted from adding the 5D5N and D362A/D367A mutations suggests that each locus acts in a relatively independent way to regulate BK gating[4,5,13].

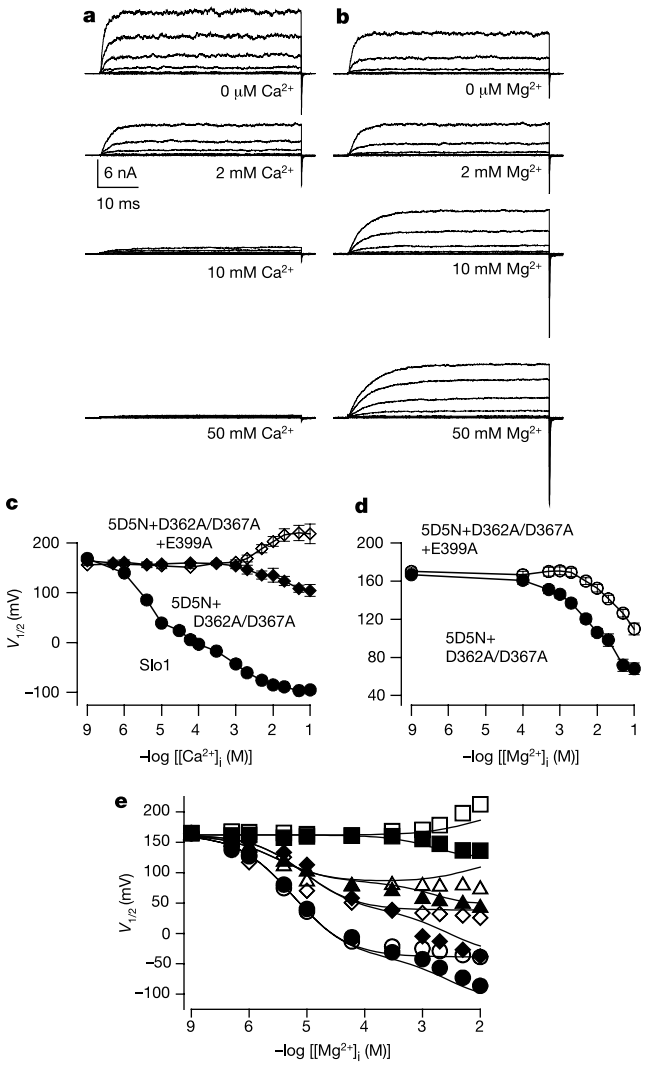

Figure 4 Mutation of all three regulatory elements produces Ca^{2+}-dependent suppression of BK current. **a** Currents resulting from the triple mutation 5D5N + D362A/D367A + E399A were activated as in Fig. 1. **b**, Mg^{2+} shifts activation of currents resulting from the triple mutation. **c**, $V_{1/2}$ is plotted versus $[Ca^{2+}]_i$ for wild type (Slo1), 5D5N + D362A/D367A and 5D5N + D362A/D367A + E399A. **d**, $V_{1/2}$ is plotted versus $[Mg^{2+}]_i$ for 5D5N + D362A/D367A, and 5D5N + D362A/D367A + E399A. **e**, An allosteric model with three independent Ca^{2+}-binding sites (equation (3)) was used to fit simultaneously the relationship between $V_{1/2}$ and $[Ca^{2+}]_i$ for all constructs. Parameter values are given in the Methods. Slo1, filled circles; E399A, open circles; 5D5N, filled diamonds; 5D5N + E399A, open diamonds; D362A/D367A, filled triangles; D362A/D367A + E399A, open triangles; 5D5N + D362A/D367A, filled squares; 5D5N + D362A/D367A + E399A, open squares.

With $[Ca^{2+}]_i$ above 1 mM, the 5D5N plus D362A/D367A mutants show an additional 50–60-mV negative shift in $V_{1/2}$, despite the lack of effect of $[Ca^{2+}]_i$ below 1 mM (Fig. 2k). This effect is similar to previously described low-affinity effects of Mg^{2+} (refs 5, 13, 25, 26) and Ca^{2+} (refs 5, 13) on BK activation. We therefore examined the ability of Mg^{2+} to produce shifts in activation in 5D5N and D362A/D367A, and the combined 5D5N plus D362A/D367A mutations. In all cases (Fig. 3a–c), the Mg^{2+}-induced shift in activation was similar to that observed in wild-type currents, indicative that the mechanism responsible for the Mg^{2+} effect was intact. This also indicates that 5D5N and D362A/D367A do not nonspecifically alter the ability of the channel to be regulated.

We next examined the role of the RCK domain on effects of millimolar concentrations of divalent cations. E399 is conserved in mammalian, fly and worm *Slo1* sequences, but not in *Slo3*. Its location on the βC sheet (Fig. 1b–c) may position it near the putative ligand-binding region. The point mutation E399A resulted in currents with reduced sensitivity only above 1 mM Ca^{2+} (Fig. 3d). Furthermore, E399A reduced the ability of Mg^{2+} to shift gating (Fig. 3g). E399A, when paired either with 5D5N (Fig 3e, h) or D362A/D367A (Fig. 3f, i), reduced the effects of both millimolar Ca^{2+} and millimolar Mg^{2+} to shift gating. In all constructs containing E399A, the $V_{1/2}$ shift resulting from increasing $[Ca^{2+}]_i$ from 1 to 100 mM is reduced by about 30–40 mV. The $V_{1/2}$ shift produced by raising $[Mg^{2+}]_i$ from 0 to 100 mM was reduced from about 110 mV to about 60 mV. The similarity of the effect of E399A in all constructs suggests that the divalent cation effect influenced by E399 acts independently of other Ca^{2+}-regulatory elements. Thus, E399 seems to define an independent lower-affinity, divalent cation-regulatory effect.

If E399 accounts for most of the additional effects of Ca^{2+} at millimolar concentrations, the triple mutant construct 5D5N plus D362A/D367A, plus E399A might be expected to abolish all Ca^{2+} sensitivity. Remarkably, currents resulting from the triple mutant did not simply exhibit insensitivity to Ca^{2+}, but were markedly suppressed as Ca^{2+} was elevated from 300 μM through to 100 mM (Fig. 4a). Although rapid block of open channels by millimolar concentrations of Ca^{2+} or Mg^{2+} is a common feature of these channels[5,13,27], such open channel block is rapidly relieved on hyperpolarization, with little steady-state block at potentials negative to −100 mV. Yet, for the triple mutant construct, currents are strongly inhibited in a voltage-independent fashion. Furthermore, the Ca^{2+}-dependent inhibition is associated with a rightward shift in the *G–V* curve compared with that in 0 Ca^{2+} (Fig. 4c). In contrast, in the triple mutation constructs Mg^{2+} still produces shifts in activation to more negative potentials (Fig. 4b).

What is the mechanism by which E399A in conjunction with mutation of the other two loci produces this suppression of current? The energetic additivity of the effects of 5D5N, D362A/D367A (Fig. 2k) and E399A (Fig. 3d–f) indicates that none of the mutations produce a nonspecific suppression in the ability of current to be regulated by Ca^{2+}. An alternative explanation is that one mutation has altered the properties of a Ca^{2+}-binding site, such that Ca^{2+} now binds more tightly to the closed channel than to the open channel. For an allosteric model in which distinct regulatory sites independently regulate the channel closed-to-open equilibria[5,7,13],

such a change in affinity will suppress current activation and shift *G–V* curves to the right. In accordance with general pharmacological principles, in the triple mutant Ca^{2+} now appears to act as an inverse agonist at one of the Ca^{2+}-binding sites. We propose that D362/D367 is probably responsible for this effect, although this will require more investigation. We have evaluated the behaviour of the wild-type currents and the various mutants in terms of a three-regulatory-site model (Fig. 4e). This model adequately accounts for many of the principal features of the behaviour of $V_{1/2}$ for all of the constructs, and supports the validity of the allosteric model of regulation of BK gating[4,5,7,13,28].

These results show that the RCK domain is critical to Ca^{2+}-dependent regulation of BK channels and participates in both higher (D362 and D367) and lower (E399) affinity effects of divalent cations. Irrespective of whether any of the critical residues in the RCK domain mediates binding with divalent cations, mutation of these residues clearly disrupts channel regulatory mechanisms that are intimately associated with specific aspects of Ca^{2+}-dependent activation. Do these loci actually reflect divalent cation binding sites? We currently consider this an attractive hypothesis. First, the principal residues are situated in positions with proximity to the nucleotide-binding sites described in other homologues, suggesting a similar regulatory role. Second, the principal residues are anionic. Third, the results suggest that a specific mutation has resulted in a change in Ca^{2+}-binding affinities, such that Ca^{2+} now acts to inhibit current activation. If a mutation simply disrupted transduction of a process regulated by a Ca^{2+}-binding site located elsewhere, a change in molecular binding affinities would not be expected. However, it remains plausible that the mutations studied here have simply disrupted the ability of the RCK domain to exert regulatory effects mediated by Ca^{2+} binding elsewhere.

The presence of multiple Ca^{2+}-dependent regulatory domains on the Slo1 α-subunit, each with different affinities for Ca^{2+}, provides a mechanism by which the broad concentration range of Ca^{2+}-dependence of BK currents can be explained. Although further analysis may reveal some linkage between the allosteric effects mediated by each regulatory element, it is remarkable that the assumption of independence in the allosteric effects of three distinct regulatory elements accounts so well for the observations. In fact, to account for the broad range of $[Ca^{2+}]_i$ over which BK channels are regulated, independence of each of the Ca^{2+}-dependent regulatory elements is required. This definition of the principal regulatory elements by which Ca^{2+} controls activation of BK currents provides a critical step towards defining how the binding of Ca^{2+} may modulate channel activation. □

Methods

Generation and expression of mutant subunits

Disruption of the Ca^{2+} bowl region was accomplished with mutation of five consecutive aspartate residues to asparagines (5D5N; mSlo1 residues 898-902)[9]. Loci for mutational analysis of the RCK domain were guided by a comparison of *Slo1* and *Slo3* sequences in or near the region between β-sheet βA and helix αA (Fig. 1c) defined in the published crystal structure of the *Escherichia coli* K^+ homologue[12]. For structural comparisons, the Slo1 amino acid sequence was threaded onto the published structure of the RCK domain of the *E. coli* K^+ channel[12]. Because of the absence of residues in the linker between helix αA and sheet βB in the *E. coli* sequence, the position of residues in this linker shown in the diagram of the BK RCK structure (Fig. 1b) is uncertain.

Construction of mutations was accomplished using standard procedures[29]. Methods of expression in *Xenopus* ooctyes were as previously described[5]. In addition to mutations involving D362, D367, D369 and E399, a number of other single point mutations involving charged residues in the RCK domain (D481A, D482A, D434A and K448A) were also examined. Similar to wild-type Slo1 currents, each of these constructs exhibit a >250-mV negative shift in $V_{1/2}$ over Ca^{2+} from 0 to 100 mM, with little difference in the shape of the pCa versus $V_{1/2}$ relationship compared to control currents.

Physiological recordings

All recordings used inside-out patches and follow procedures in standard use in our laboratory[5,30]. The pipette extracellular solution was 140 mM potassium methanesulphonate, 20 mM KOH, 10 mM HEPES, 2 mM $MgCl_2$ (pH 7.0). Test solutions bathing the cytoplasmic face of the patch membrane contained 140 mM potassium methanesulphonate, 20 mM KOH, 10 mM HEPES (pH 7.0), and one of the following: 5 mM EGTA (for nominally 0 Ca^{2+}, 0.5 and 1 μM Ca^{2+} solutions), 5 mM HEDTA (for 4 and 10 μM Ca^{2+} solutions), or no added Ca^{2+} buffer (for 30 μM and higher Ca^{2+}). The methods of calibration and preparation of Mg^{2+} solutions have been described previously[5,30]. Excised patches were bathed with constantly flowing solutions of defined Ca^{2+} from a multibarrel local application system.

Conductance–voltage (*G–V*) curves were generated from tail currents following standard procedures[5]. Families of *G–V* curves represent averages from a set of patches at specific $[Ca^{2+}]_i$. For each patch, *G–V* curves were fit with

$$G(V) = G_{max}/(1 + \exp^{(V - V_{1/2})/k}) \quad (1)$$

to provide estimates of $V_{1/2}$, the voltage of half activation, and k, the slope factor describing the voltage-dependence of the closed–open equilibrium. Estimates of the $V_{1/2}$ value for a given ionic condition represent the mean value for a set of five to ten individual patches. In all cases, error bars show s.e.m. In Fig. 3, for comparison of the magnitude of $V_{1/2}$ shifts, $V_{1/2}$ values for each construct were adjusted so that the values at 0 mM were identical. For all constructs, absolute $V_{1/2}$ values at 0 mM ranged from within about 20 mV, a range similar to that observed for different sets of patches from the same construct. Experiments were at room temperature (21–24 °C). Most salts and chemicals were from Sigma.

Allosteric models of BK current activation

For an allosteric model in which membrane voltage and one or more distinct ligand-binding sites all independently regulate the transition between closed and open conformations, the energy provided by each regulatory site is additive in activating the channel[7]. Such a model predicts that the shift in $V_{1/2}$ for a single divalent cation-binding site follows the following relationship for the case that there is one Ca^{2+}-binding site on each of the four BK α-subunits[5,13].

$$V_{1/2} = V_{1/2}(0) + \frac{4kT}{ze}\left\{\ln\left[\frac{1 + \frac{[Ca^{2+}]_i}{K_{C1}}}{1 + \frac{[Ca^{2+}]_i}{K_{O1}}}\right]\right\}, \quad (2)$$

where $V_{1/2}(0)$ corresponds to activation $V_{1/2}$ at 0 Ca^{2+}, K_{C1} and K_{O1} correspond to the Ca^{2+} affinity of the closed and open channel, respectively, k is Boltzmann's constant and T is absolute temperature. For three distinct, independent regulatory elements, $V_{1/2}$ is predicted to shift in accordance with the following relationship:

$$V_{1/2} = V_{1/2}(0,0) + \frac{4kT}{ze}\left\{\ln\left(\frac{1 + \frac{[Ca^{2+}]_i}{K_{C1}}}{1 + \frac{[Ca^{2+}]_i}{K_{O1}}}\right) + \ln\left(\frac{1 + \frac{[Ca^{2+}]_i}{K_{C2}}}{1 + \frac{[Ca^{2+}]_i}{K_{O2}}}\right) + \ln\left(\frac{1 + \frac{[Ca^{2+}]_i}{K_{C3}}}{1 + \frac{[Ca^{2+}]_i}{K_{O3}}}\right)\right\} \quad (3)$$

Thus, the shift in $V_{1/2}$ for each regulatory element is additive with the contributions of the other regulatory elements. Equation (3) was used to fit the relationship between $V_{1/2}$ and Ca^{2+} for all constructs (Fig. 4c). All points were fitted simultaneously. Estimates for Ca^{2+} binding affinities were: for the Ca^{2+} bowl, $K_{C1} = 4.5 \pm 1.7$ μM and $K_{O1} = 2.0 \pm 0.7$ μM; for D362/D367, $K_{C2} = 17.2 \pm 4.0$ μM and $K_{O2} = 4.6 \pm 1.0$ μM; and for E399, $K_{C3} = 4.1 \pm 3.5$ mM and $K_{O3} = 1.8 \pm 1.2$ mM. With mutation to D362A/D367A, $K_{C2} = 6.6$ mM and $K_{O2} = 10.7$ mM, accounting for the inhibitory effects of Ca^{2+}. Values above 10 mM were not included in the fit.

Received 16 April; accepted 19 June 2002; doi:10.1038/nature00956.

1. Barrett, J. N., Magleby, K. L. & Pallotta, B. S. Properties of single calcium-activated potassium channels in cultured rat muscle. *J. Physiol. (Lond.)* **331,** 211–230 (1982).
2. Moczydlowski, E. & Latorre, R. Gating kinetics of Ca^{2+}-activated K^+ channels from rat muscle incorporated into planar lipid bilayers. Evidence for two voltage-dependent Ca^{2+} binding reactions. *J. Gen. Physiol.* **82,** 511–542 (1983).
3. Cox, D. H., Cui, J. & Aldrich, R. W. Allosteric gating of a large conductance Ca-activated K^+ channel. *J. Gen. Physiol.* **110,** 257–281 (1997).
4. Cox, D. & Aldrich, R. Role of the β1 subunit in large-conductance Ca^{2+}-activated K^+ channel gating energetics. Mechanisms of enhanced Ca^{2+} sensitivity. *J. Gen. Physiol.* **116,** 411–432 (2000).
5. Zhang, X., Solaro, C. & Lingle, C. Allosteric regulation of BK channel gating by Ca^{2+} and Mg^{2+} through a non-selective, low affinity divalent cation site. *J. Gen. Physiol.* **118,** 607–635 (2001).
6. Cui, J., Cox, D. H. & Aldrich, R. W. Intrinsic voltage dependence and Ca^{2+} regulation of mslo large conductance Ca-activated K^+ channels. *J. Gen. Physiol.* **109,** 647–673 (1997).
7. Cui, J. & Aldrich, R. W. Allosteric linkage between voltage and Ca^{2+}-dependent activation of BK-type mslo1 K^+ channels. *Biochemistry* **39,** 15612–15619 (2000).
8. Horrigan, F. T., Cui, J. & Aldrich, R. W. Allosteric voltage gating of potassium channels I. Mslo ionic currents in the absence of Ca^{2+}. *J. Gen. Physiol.* **114,** 277–304 (2002).
9. Schreiber, M. & Salkoff, L. A novel calcium-sensing domain in the BK channel. *Biophys. J.* **73,** 1355–1363 (1997).
10. Schreiber, M., Yuan, A. & Salkoff, L. Transplantable sites confer calcium sensitivity to BK channels. *Nature Neurosci.* **2,** 416–421 (1999).
11. Bian, S., Favre, I. & Moczydlowski, E. Ca^{2+}-binding activity of a COOH-terminal fragment of the *Drosophila* BK channel involved in Ca^{2+}-dependent activation. *Proc. Natl Acad. Sci. USA* **98,** 4776–4781 (2001).
12. Jiang, Y., Pico, A., Cadene, M., Chait, B. T. & MacKinnon, R. Structure of the RCK domain from the *E. coli* K^+ channel and demonstration of its presence in the human BK channel. *Neuron* **29,** 593–601 (2001).
13. Shi, J. & Cui, J. Intracellular Mg^{2+} enhances the function of BK-type Ca^{2+}-activated K^+ channels. *J. Gen. Physiol.* **118,** 589–606 (2001).
14. Shao, L. R., Halvorsrud, R., Borg-Graham, L. & Storm, J. F. The role of BK-type Ca^{2+}-dependent K^+ channels in spike broadening during repetitive firing in rat hippocampal pyramidal cells. *J. Physiol.* **521(1),** 135–146 (1999).
15. Jones, E. M., Gray-Keller, M. & Fettiplace, R. The role of Ca^{2+}-activated K^+ channel spliced variants in the tonotopic organization of the turtle cochlea. *J. Physiol.* **518,** 653–665 (1999).
16. Adelman, J. P. *et al.* Calcium-activated potassium channels expressed from cloned complementary DNAs. *Neuron* **9,** 209–216 (1992).

17. Butler, A., Tsunoda, S., McCobb, D. P., Wei, A. & Salkoff, L. mSlo, a complex mouse gene encoding "maxi" calcium-activated potassium channels. *Science* **261,** 221–224 (1993).
18. Shen, K. Z. *et al.* Tetraethylammonium block of Slowpoke calcium-activated potassium channels expressed in *Xenopus* oocytes: evidence for tetrameric channel formation. *Pflugers Arch.* **426,** 440–445 (1994).
19. Meera, P., Wallner, M., Song, M. & Toro, L. Large conductance voltage- and calcium-dependent K^+ channel, a distinct member of voltage-dependent ion channels with seven N-terminal transmembrane segments (S0-S6), an extracellular N terminus, and an intracellular (S9-S10) C terminus. *Proc. Natl Acad. Sci. USA* **94,** 14066–14071 (1997).
20. Wei, A., Solaro, C., Lingle, C. & Salkoff, L. Calcium sensitivity of BK-type KCa channels determined by a separable domain. *Neuron* **13,** 671–681 (1994).
21. Jiang, Y. *et al.* Crystal structure and mechanism of a calcium-gated potassium channel. *Nature* **417,** 515–522 (2002).
22. Bellamacina, C. R. The nicotinamide dinucleotide binding motif: a comparison of nucleotide binding proteins. *FASEB J.* **10,** 1257–1269 (1996).
23. Schreiber, M. *et al.* Slo3, a novel pH-sensitive K^+ channel from mammalian spermatocytes. *J. Biol. Chem.* **273,** 3509–3516 (1998).
24. Moss, B. L. & Magleby, K. L. Gating and conductance properties of BK channels are modulated by the S9-S10 tail domain of the alpha subunit. A study of mSlo1 and mSlo3 wild-type and chimeric channels. *J. Gen. Physiol.* **118,** 711–734 (2001).
25. Golowasch, J., Kirkwood, A. & Miller, C. Allosteric effects of Mg^{2+} on the gating of Ca^{2+}-activated K^+ channels from mammalian skeletal muscle. *J. Exp. Biol.* **124,** 5–13 (1986).
26. Oberhauser, A., Alvarez, O. & Latorre, R. Activation by divalent cations of a Ca^{2+}-activated K^+ channel from skeletal muscle membrane. *J. Gen. Physiol.* **92,** 67–86 (1988).
27. Ferguson, W. B. Competitive Mg^{2+} block of a large-conductance, Ca^{2+}-activated K^+ channel in rat skeletal muscle. Ca^{2+}, Sr^{2+}, and Ni^{2+} also block. *J. Gen. Physiol.* **98,** 163–181 (1991).
28. Rothberg, B. S. & Magleby, K. L. Gating kinetics of single large-conductance Ca^{2+}-activated K^+ channels in high Ca^{2+} suggest a two-tiered allosteric gating mechanism. *J. Gen. Physiol.* **114,** 93–124 (1999).
29. Xia, X. M., Ding, J. P. & Lingle, C. J. Molecular basis for the inactivation of Ca^{2+}- and voltage-dependent BK channels in adrenal chromaffin cells and rat insulinoma tumour cells. *J. Neurosci.* **19,** 5255–5264 (1999).
30. Lingle, C., Zeng, X.-H., Ding, J.-P. & Xia, X.-M. Inactivation of BK channels mediated by the N-terminus of the β3b auxiliary subunit involves a two-step mechanism: possible separation of binding and blockade. *J. Gen. Physiol.* **117,** 583–605 (2001).

Acknowledgements

We thank the members of our laboratory for encouragement and assistance during this work and L. Lavack for preparation and care of oocytes. We thank J. H. Steinbach, J. Nerbonne and L. Salkoff for discussions and comments on the manuscript. We also thank the Department of Anesthesiology, Washington University School of Medicine, for material support.

Competing interests statement

The authors declare that they have no competing financial interests.

Correspondence and requests for materials should be addressed to C.J.L. (e-mail: clingle@morpheus.wustl.edu).

A bacteriolytic agent that detects and kills *Bacillus anthracis*

Raymond Schuch, Daniel Nelson & Vincent A. Fischetti

Laboratory of Bacterial Pathogenesis and Immunology, The Rockefeller University, New York, New York 10021, USA

The dormant and durable spore form of *Bacillus anthracis* is an ideal biological weapon of mass destruction[1,2]. Once inhaled, spores are transported by alveolar macrophages to lymph nodes surrounding the lungs, where they germinate; subsequent vegetative expansion causes an overwhelming flood of bacteria and toxins into the blood, killing up to 99% of untreated victims. Natural and genetically engineered antibiotic-resistant bacilli amplify the threat of spores being used as weapons, and heighten the need for improved treatments and spore-detection methods after an intentional release. We exploited the inherent binding specificity and lytic action of bacteriophage enzymes called lysins for the rapid detection and killing of *B. anthracis*. Here we show that the PlyG lysin, isolated from the γ phage of *B. anthracis*, specifically kills *B. anthracis* isolates and other members of the *B. anthracis* 'cluster' of bacilli *in vitro* and *in vivo*. Both vegetative cells and germinating spores are susceptible. The lytic specificity of PlyG was also exploited as part of a rapid method for the identification of *B. anthracis*. We conclude that PlyG is a tool for the treatment and detection of *B. anthracis*.

Bacteriophage lysins are lytic agents used by double-stranded DNA (dsDNA) phages to coordinate bacterial host lysis with completion of viral assembly[3,4]. Late in infection, lysin translocates from the cytoplasm into the cell-wall matrix, where it rapidly hydrolyses covalent bonds essential for peptidoglycan integrity, causing bacterial lysis and concomitant release of progeny phages. Lysin family members are often chimaeric proteins, consisting of a usually well-conserved catalytic domain fused to a largely divergent specificity or binding domain[4,5]. High-affinity binding (the affinity constant $K_A = 3–6 \times 10^8$, similar to affinity-matured antibodies) is directed towards species- or strain-specific cell-wall carbohydrates that are often essential for viability, thus implying that intrinsic lysin resistance could be rare. Lysins have not previously been investigated as a means for bacterial control, although we have demonstrated efficient 'lysis from without' of pathogenic streptococci in the mouse nasopharynx using purified streptococcal phage lysins[6,7]. On the basis of these findings, we thought that lysins might be able to deliver a rapid and specific lethal action to any particular bacterial pathogen, not just streptococci. The main requirement for developing lysins, as such, is a dsDNA phage specific for the pathogen of interest to serve as a lysin source. We investigated this possibility with a dsDNA phage specific for the biowarfare agent *B. anthracis*.

The dsDNA phages of *B. anthracis* form a homogeneous family[8]. We chose the γ phage as a lysin source because of its specificity for *B. anthracis* and its usage by the US Centers for Disease Control and Prevention (CDC, Atlanta, Georgia) for identification of this pathogen[2,9]. It is known that γ phages infect most *B. anthracis* isolates, including some rare *Bacillus cereus* strains that could represent *B. anthracis* cured of its virulence plasmid or an environmental reservoir of potential progenitors[10]. Isolates of RSVF1 (streptomycin-resistant *B. cereus* strain 4342 from the American Type Culture Collection, ATCC) and *B. anthracis* are monomorphic at multiple allozyme loci, and therefore are part of the same highly related cluster of isolates within the *B. cereus* lineage[11]. Consistent with this, we found that RSVF1 was sensitive to the γ phage (Table 1) and displayed several other features typical of *B. anthracis*: matt colony morphology, filamentous structure, lack of motility, and characteristic sequences in the hypervariable *vrrA* locus (data not shown). For these reasons, RSVF1 is an appropriate representative of the γ-phage-sensitive *B. anthracis* cluster of *B. cereus* for use in this study.

An expression library of γ phage proteins was screened for agents capable of lysing RSVF1 'from without'. Each lytic clone identified contained a 702-base-pair (bp) γ open reading frame (ORF) encoding a product that is homologous to *N*-acetylmuramoyl-L-alanine amidases (amidases), a class of phage lysins (Fig. 1a). The homology was restricted to the catalytic amino-terminal halves, and absent in the cell-wall-specific carboxy-terminal binding domains[4,5]. Recombinant γ lysin (called PlyG, for phage lysin γ) was purified to homogeneity by column chromatography (Fig. 1b). Gel filtration confirmed a predicted relative molecular mass of about 27,000 (M_r 27K), and suggested that PlyG acts as a monomer and is not proteolytically processed.

To evaluate activity and specificity, 0.5 U of PlyG was initially added in drops to bacterial lawns of RSVF1 (Fig. 1c) and isolates of *B. anthracis* gathered worldwide as well as other bacilli from the *B. cereus* lineage (*B. cereus* and *Bacillus thuringiensis*) and other Gram-positive genera (Table 1). RSVF1 was the only *B. cereus* strain found to be as sensitive to PlyG killing (and sensitive to the γ phage) as the diverse set of *B. anthracis* isolates (Table 1). *B. cereus* ATCC 10987, a strain closely related to *B. anthracis*[11], was slightly susceptible to

